Thermomechanical Processing Environment and Morphology Development of a Thermotropic Polymer Liquid Crystal

Júlio C. Viana,[1] Ricardo Simões,[1,3] João F. Mano,[2] Maria. J. Oliveira,[1] Zlatan Z. Denchev,[1] Witold Brostow,[3] António M. Cunha[1]

[1]*IPC - Institute for Polymers and Composites, Department of Polymer Engineering, University of Minho, 4800-058 Guimaraes, Portugal*
[2]*3B's Research Group in Biomaterials, Biodegradable, Biomimetics, Department of Polymer Engineering, University of Minho, 4800-058 Guimaraes, Portugal*
[3]*Laboratory of Advanced Polymers & Optimized Materials (LAPOM), Department of Materials Science and Engineering, University of North Texas, Denton, Texas 76203-5310*

Received 4 January 2007; accepted 12 May 2007
DOI 10.1002/app.30087
Published online 30 October 2009 in Wiley InterScience (www.interscience.wiley.com).

ABSTRACT: We have studied a longitudinal polymer liquid crystal consisting of poly(ethylene terephthalate) (PET) and *p*-hydroxybenzoic acid, namely PET/0.6PHB, where 0.6 is the mole fraction of the second component. The material was injection molded with systematic variations of the melt and mold temperatures and injection flow rate using design of experiments based on a Taguchi orthogonal array. Thermomechanical environment defined by local melt temperatures and shear rates and stresses imposed during processing was estimated by computer simulations of the mold-filling phase. The morphology of the moldings was characterized by optical and scanning electronic microscopy, wide- and small-angle X-ray scattering, and differential scanning calorimetry. An analysis of variance approach identified the significant processing variables and their contributions to variations of morphological parameters. The processing environment affects strongly the melt viscosity, and there is a strong thermomechanical coupling. The result is a complex multilaminated and hierarchical microstructure, whose morphological features are very sensitive to the processing conditions. Relationships between local thermomechanical variables (rather than global ones) and the morphological parameters are established. © 2009 Wiley Periodicals, Inc. J Appl Polym Sci 115: 2991–3004, 2010

Key words: polymer liquid crystal; injection molding; processing; thermomechanical environment; morphology

INTRODUCTION

Polymer liquid crystals (PLCs) are high performance polymers and exhibit an advantageous combination of properties, particularly in applications requiring high thermal and mechanical performance, high chemical resistance, and high dimensional stability. However, their high cost has limited the widespread use of these polymers, promoting their blending with thermoplastics engineering polymers.[1–3]

Longitudinal (or main-chain) PLCs are copolymers comprised of rigid liquid crystalline (LC) sequences connected to flexible sequences by chemical bonds. The rigid mesogenic groups are exclusively in the main chain and are oriented parallel to it (so-called α-type PLC).[3–6] This segmental nature allows easy orientation of the rigid segments under external applied fields, whether electric, magnetic, or mechanical.[7–13] In fact, their thermotropic character allows them to be transformed by melt processing techniques, such as injection molding, because of their low viscosity resultant from the easy orientation of the rigid segments in the flowing melt. Because of high relaxation times of PLCs, the orientation induced by the flow cannot easily relax during subsequent cooling, leading to highly oriented structures (self-reinforced polymers) with exceptional mechanical behavior and highly anisotropic character.[14,15] Methods for successful prediction of long-term performance of PLCs from short-term tests have been developed.[16,17]

In a PLC, the rigid phase is inhomogeneously dispersed throughout the material forming a

Correspondence to: J. C. Viana (jcv@dep.uminho.pt).
Contract grant sponsor: DESY and the European Commission (under HASYLAB Project DESY-D-II-05-101 EC).
Contract grant sponsor: Robert A. Welch Foundation, Houston; contract grant numbers: B-1203, FP6, RII3-CT-2004-506008.
Contract grant sponsor: FCT - Portuguese Foundation for Science and Technology, Lisbon (through the POCTI and FEDER programmes).

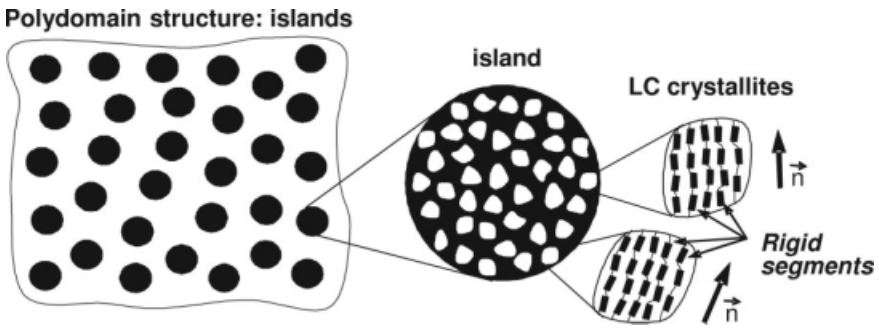

Figure 1 Polydomain hierarchical structure of a PLC (*n* is the orientation director).

hierarchical poly-domain structure[1,18]; Figure 1. The PLC tends to form spherical or ellipsoidal aggregates of LC-rich phase which are called islands.[1,18,19]

The islands constitute of smaller quasispherical shape LC crystallites connected by flexible chain segments. Wide-angle X-ray scattering (WAXS) results show that the LC crystallites (with dimensions of several nm) are mostly composed of highly oriented and packed rigid sequences of the macromolecular chains.[18,19] However, although each LC crystallite is highly oriented, the different crystallites are randomly oriented inside an island, so that no preferred orientation exists inside the islands.[15] The rigid phase is easily oriented during processing forming highly oriented structures. Shear and extensional stress fields have different effects on the morphology developed in PLCs. The former will result in a tumbling flow originating highly oriented sheet-like structures. An extensional flow leads to the development of fiber-like structures.[20]

Injection molding is an attractive technology for the production of large series of parts with a complex geometry. During processing, the polymer melt is subjected to a complex thermomechanical environment that constrains the respective morphological development. In the case of PLCs, with high shear and elongational fields and fast cooling rates, a complex highly heterogeneous laminated microstructure is formed, which is composed of several layers featuring distinct textures and states of molecular orientation.[21–24] Elongational viscosity of several PLC blends shows that the PLC constituent causes channelling of the flexible polymer[25] and thus its orientation along the PLC—this effect is predicted theoretically by an extension of the Flory statistical-mechanical theory of PLCs.[26]

At the micrometric level, a five-layer laminated microstructure is normally formed: two external skins, two intermediate zones, and a central core region. The skin and the intermediate zone can be further discriminated and more sublayers can be identified. The number of identifiable layers depends on the thickness of the molding and the criteria established by the observer. The skin layer exhibits a high level of molecular orientation. This feature, combined with the lack of chain entanglements, makes the skin layer easy to delaminate. In the core region, the melt experiences a tumbling flow of LC islands, resulting in molecular orientation along the flow lines. Studies of the morphology development of injection-molded PLCs has been based on the traditional approach of directly relating the global processing conditions (e.g., temperatures, velocities, molding thickness) to the morphological parameters.[23,24,27,28] This does not support the establishment of universally valid processing-morphology relationships, which are molding geometry and injection molded machine dependent. It does not support a predictive effort. Our approach—used in the present work—is different; we believe that these types of relationships must be established locally, relating the local thermomechanical environment to the developed morphology. The processing-morphology relationships are, therefore, of a more general character, independent of selected injection molding machine and molding geometry.

This work investigated the structure development of an injection-molded thermotropic PLC. The local thermomechanical environment is assessed by computer simulations of the mold-filling phase. The morphology developed by the injection-molded PLC specimens is characterized by several structure-sensitive experimental techniques including the following: scanning electronic microscopy, differential scanning calorimetry, wide-, and small-anlge X-ray scattering. The relationships between the local processing thermomechanical variables and the morphological parameters are then established. A study of the relationships between the developed morphology and the mechanical behavior of injection-molded PLCs will be described in a later article. It is expected that the morphology developed during processing, because of the imposed thermomechanical environment, will affect the mechanical properties of the injection-molded PLCs. This was demonstrated before by molecular dynamics computer simulations of PLCs comprised of amorphous polymeric chains and a rigid LC phase dispersed

throughout the flexible matrix in the form of quasi-spherical islands. Simulation results indicate that both the LC concentration and spatial distribution influence the response of the material.[29,30] Furthermore, the presence of the rigid LC phase affects the predominant molecular deformation mechanisms,[31] and the crack formation and propagation phenomena.[29] On the other hand, experiments tell us that other morphological features—such as the skin-core ratio in injection-molded materials—influence the final macroscopic properties.[32]

EXPERIMENTAL

Material and specimen geometry

The material is a longitudinal PLC: a copolyester comprised of 0.6 mole fraction of *p*-hydroxybenzoic acid (PHB) and 0.4 mole fraction of poly(ethylene terephtalate) (PET), referred to as PET/0.6PHB. It was purchased from Unitika, Kyoto, Japan, under the commercial name of Rodrun LC-3000. PET/0.6PHB has a density = 1.4 g cm^{-3} and a melting temperature = 200°C.[33] Above that temperature, we have a smectic E phase coexisting with the isotropic liquid. Upon further heating, we have a 3-phase system (smectic E, smectic B, and isotropic liquid), then a different 2-phase system (smectic B and isotropic liquid) until the clearing temperature $\approx$ 420°C is reached.[33]

The molded specimens are tensile dumbbell-like bars 60-mm long with 20 mm of reference length and uniform rectangular cross-section (4 $\times$ 2 mm^2). The tab gate was located laterally in the middle of the specimen head.

Processing and thermomechanical environment

Molding programme

The molding program includes systematic variations of three processing variables: melt and mold temperature, T_{inj} and T_w, respectively, and injection flow rate, Q_{inj}. These were varied in three levels (1, minimum; 2, medium; and 3, maximum) following a design of experiments (DOE) plan based on a Taguchi orthogonal matrix (L9). This plan ensures that the effects of each processing variable can be analyzed independently of each other. Table I lists the values of the processing variables for each processing run. All the other processing parameters were kept constant. The order of the processing runs was randomized to avoid blocking effects.

The PLC material pellets were dried at 100°C during 12 h before molding. They were then molded in a Klocker-Ferromatic FM 20 injection molding machine. In each run, the weight of the molded samples was statistically controlled.

TABLE I
Molding Program Based on a L9 Taguchi Orthogonal Matrix

Run	T_{inj} (°C)	T_w (°C)	Q_{inj} (cm^3/s)/t_{inj} (s)
R1	220	20	4.9/1.00
R2	220	40	18.4/0.45
R3	220	60	27.0/0.10
R4	250	20	27.0/0.10
R5	250	40	4.9/1.00
R6	250	60	18.4/0.45
R7	280	20	18.4/0.45
R8	280	40	27.0/0.10
R9	280	60	4.9/1.00

T_{inj}, melt temperature; T_w, mold temperature; Q_{inj}, injection flow rate; t_{inj}, injection time.

Thermomechanical environment characterization

The thermomechanical environment imposed upon the melt during processing was estimated by computer modeling of the mold-filling stage using a commercial Moldflow package. A thermotropic PLC such as Rodrun LC3000 shows a complex rheological behavior because of its flexible-rigid segmental nature and polydomain structure. The rheological flow curves exhibit distinct behavior depending on the selected temperature,[34] evidencing a strong dependence of the viscosity upon the temperature. In the high shear rates regime (10^1 to 10^3 s^{-1}), a temperature-dependent shear thinning behavior can be assumed. In this study, the experimental viscosity data reported elsewhere[34] was used and fitted to a power-law equation:

$$\eta = 1.060 \times 10^{14} \dot{\gamma}^{-0.41} e^{-0.199T} \quad (1)$$

with T in °C. This simple constitutive model was used in the mold-filling simulations, despite its oversimplification in describing the rheological behavior of the material, which may lead to a less accurate characterization of the thermomechanical environment. The mold-filling simulations allowed the estimation of the through-the-thickness temperature, shear rate, and stress profiles. These profiles were characterized, respectively, by the bulk temperature, T_b, the maximum shear rate, $\dot{\gamma}_{max}$ and the shear stress at the solid/liquid interface, τ_w. A cooling index, Y, was defined as[32,35–37]:

$$Y = \frac{T_b - T_t}{T_b - T_w} \quad (2)$$

where T_t is a transition temperature (a constant value of T_t = 200°C was used). Y characterizes the thermal level of the moldings: a high Y corresponds to a slower cooling process.

Morphological characterization

Scanning electronic microscopy

The fracture surfaces of the tensile specimens were observed in a scanning electronic microscope (SEM) Leica Cambridge LS360. The samples were previously sputtered with a thin conductive layer of gold. Two magnifications were used: ×30 for observing the overall microstructure of the injection moldings and ×5,000 for observing the intermediate layer. The microstructure of the moldings was evaluated by measuring the thickness of each layer in their multilayered structure. Measurements were made under the lower magnification SEM micrographs using an image analyser software.

Differential scanning calorimetry

Differential scanning calorimetry (DSC) scans were performed in a PerkinElmer DSC-7 apparatus in heating. Both experiments and calibrations (temperature and heat flow) were performed with indium standard at 20°C/min. Sample cross-sections of 14–20 mg were cut from the central zone of the specimens. One sample per processing run was used. For processing Run 1, the DSC experiment was repeated for three different specimens. Experimental scatter of 4.9, 0.7, and 14.6% was found, respectively, for the enthalpy of melting H_m, the glass transition temperature T_g, and the heat capacity change upon melting ΔC_p (this error was assumed as equally dispersed within the other runs).

Wide- and small-angle X-ray scattering

The crystalline phase morphology of the moldings was studied by X-ray synchrotron radiation source (transmission mode), generated at the Soft Condensed Matter beam line (A2 polymer), HASYLAB, at DESY, Hamburg, Germany (Gc with the wavelength of $\lambda = 0.15$ nm). The injection-molded specimens were placed vertically (flow direction in the vertical) and perpendicularly to the incident X-ray beam. The experimental set-up allowed for the simultaneous acquisition of both wide-angle (WAXS) and small-angle X-ray (SAXS) bidimensional scattering patterns. For both techniques only one specimen per processing run was used.

The WAXS patterns were recorded on a phosphorus-based image plate after the exposure time of 60 s. The specimen-to-detector distance was 22 cm. The $\theta-2\theta$ scattering scans for the equatorial reflection and the azimuthal angle scans for the mesogenic group reflection (highest intensity reflection arc) were obtained from the 2D WAXS patterns. Both these curves were corrected for background scattering and beam-intensity and normalized with respect to the specimen thickness and accumulation time. In the $\theta-2\theta$ scans the scattering angle coordinate was calibrated using a semi-crystalline PET sample.

The level of orientation (or second-order orientation function), s, was calculated from the angular intensity distribution $I(\phi)$, using the Herman's orientation function as discussed by Gedde and Wiberg[15]:

$$s = \frac{1}{2}\left(3\langle\cos^2\phi\rangle - 1\right) \tag{3}$$

where is the angle between the axis of the average mesogen direction (director) and the preferred direction of the nematic phase. The angle brackets mean the averaging over the azimuthal angle, i.e.,

$$\langle\cos^2\phi\rangle = \frac{\int_0^{\pi/2} I(\phi)\cos^2\phi\sin\phi\,d\phi}{\int_0^{\pi/2} I(\phi)\,\sin\phi\,d\phi} \tag{4}$$

where $I(\phi)$ is the scattered intensity of the mesogenic reflection at the azimuthal angle.

The parameter s can also be obtained by other routes, for instance by proton and deuterium nuclear magnetic resonance as described by Arrighi et al.[38] It follows from the definition of the angle that $s = 1$ for a system comprising molecules perfectly aligned in the flow direction. As already noted, given a highly layered configuration of injection-molded PLC, the use of a single global parameter to characterize the orientation state may be misleading. Tentatively, we might use a global through-the-thickness value of s as a measure of the mean orientation averaged over the thickness of the sample.

The SAXS reflections were recorded in a MARCCD detector, from which bidimensional patterns were obtained. The specimen-to-detector distance was 202 cm. The same exposure time was used as in the WAXS analysis. From these 2D patterns the intensity-scattering vector scans (in the meridional/flow direction) were calculated. Again, and as before, the intensity values were corrected from background scattering and beam intensity, and normalized with respect to the specimen thickness and exposure time. In the SAXS experiments, the scattering vector coordinate was calibrated by a rat tendon tail standard.

RESULTS

Thermomechanical environment characterization

Table II lists the computed values of the variables selected to characterize the thermomechanical environment associated with the experimental programme. The processing conditions resulted in a considerable variation of the shear stress and shear rate, also due to the high dependence of the

TABLE II
Computed Thermomechanical Variables

Run	T_b (°C)	τ_w (kPa)	$\dot{\gamma}_{max}$ (s^{-1})
R1	219.3	70.0	3.82×10^2
R2	220.3	57.4	8.69×10^2
R3	220.8	67.7	3.98×10^3
R4	249.9	3.20	3.97×10^3
R5	247.7	3.68	3.81×10^2
R6	249.3	2.55	8.62×10^2
R7	279.1	8.37×10^{-2}	8.62×10^2
R8	279.9	9.46×10^{-2}	3.98×10^3
R9	277.6	1.18×10^{-1}	3.80×10^2
Variation[a] (%)	27.6	8.35×10^4	9.95×10^3

T_b, bulk temperature; $\dot{\gamma}_{max}$, maximum shear rate; τ_w, shear stress at the solid/melt interface.
[a] Variation = [(maximum value)-(minimum value)]/(minimum value) × 100.

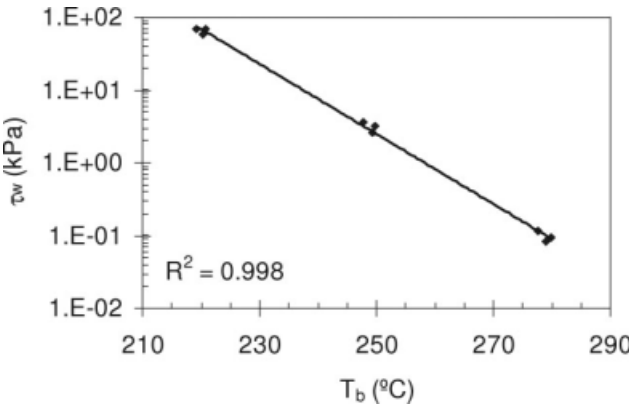

Figure 2 Relationship between the wall shear stress, τ_w, and the bulk temperature, T_b, for all the moldings evidencing a strong thermo-mechanical coupling (the solid line is the fitting of the data with $\tau_w = 2.55 \times 10^{12} e^{-0.111 T_b}$ equation (R^2 is the coefficient of correlation).

rheological behavior on the temperature and shearing levels. The values of T_b are only dependent upon the melt temperature, both temperatures being very similar. The bulk temperature increases linearly with the melt temperature. The highest variations were found in the shear stress, which is influenced mostly by the melt temperature. This is a consequence of the strong temperature dependence of the melt viscosity. The shear rate shows a two-decade amplitude of variation and is affected only by the injection flow rate: an increment on the injection flow rate induces a strong increase on the shear rate, as would be expected. In this shear rate range (10^2 to 10^3 s^{-1}), the temperature and shear rate dependence of the viscosity were assumed to be well described by a power law model with an Arrhenius thermal dependence.

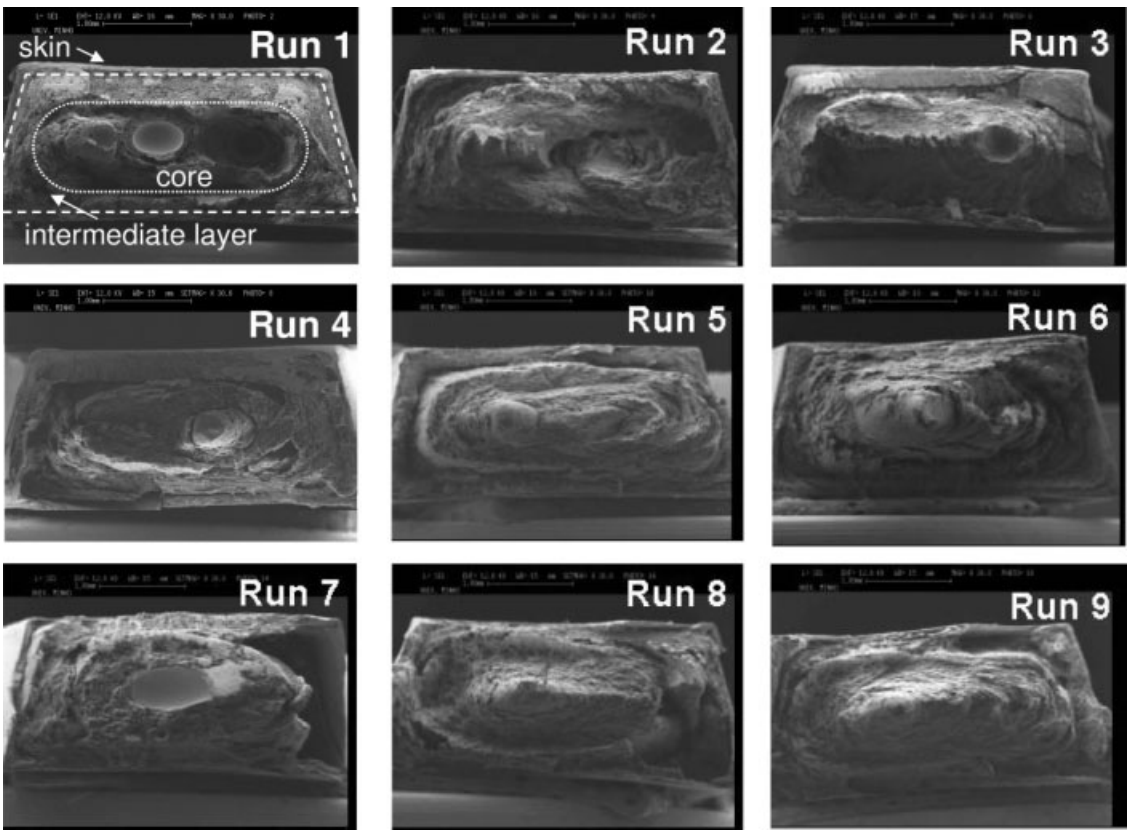

Figure 3 Effect of the processing variables (see Table I) on the microstructure of the moldings: SEM micrographs of the fracture surfaces.

A strong thermal and mechanical coupling is evidenced during processing, as depicted in Figure 2, and already anticipated from the data in Table II. In fact, the data can be divided in three groups accordingly to T_b and τ_w ranges. This thermomechanical coupling strongly determines and limits the morphology development in injection molding.[35–37]

Morphological characterization by SEM

Figure 3 depicts the SEM micrographs of the fracture surfaces of all the tensile specimens. The processing conditions induce distinct patterns in the fracture surfaces.

The overall trend is the formation of a five-layer laminate composed of a very thin external layer, a large intermediate zone and an internal core, as illustrated in Figure 3 (Run 1). The thinner skin layer is developed during the filling stage as the hot material enters in contact with the cold mold wall, and its thickness is determined by the heat transfer conditions.[23] In the core region the melt experiences a tumbling flow of the poly-domains. This results in molecular orientation along the flow lines of this tumbling flow.[19,23] The fracture surfaces follow this imposed orientation, giving rise to parabolic patterns seen in the cores of the fracture specimens. In the intermediate layer, the molecular chains can be highly oriented in the flow direction. This layer can be therefore easily delaminated, creating visible holes (e.g., Run 7 in Fig. 3). A magnified view of these intermediate zones is presented in Figure 4 for selected processing runs.

For processing condition R2 it is possible to observe some spherical domains that were not deformed during the mechanical drawing. These aggregates are more evident for the low-melt temperature moldings (Runs 1 to 3), suggesting a weak coupling between these aggregates. Conversely, condition R8 shows a highly deformed structure, typical of samples molded at the highest melt temperature (Runs 7 to 9). In this case, the stress is better transferred to the aggregates which are able to deform, resulting in high local plasticity. For condition R5, some fibrillar-like structures can be observed (similarly also in Run 6). This type of morphology appears as intermediate with respect to those referred to above. The thicknesses of the layers were measured from the SEM micrographs. The skin layer is very small (c.a. 11% of the total molding thickness) and the measurements were not very accurate. For that reason, only two layers were considered: a highly oriented external layer (corresponding to the sum of the thickness of the skin and intermediate layers, S_i; see Fig. 3) and a central core layer, C_a.

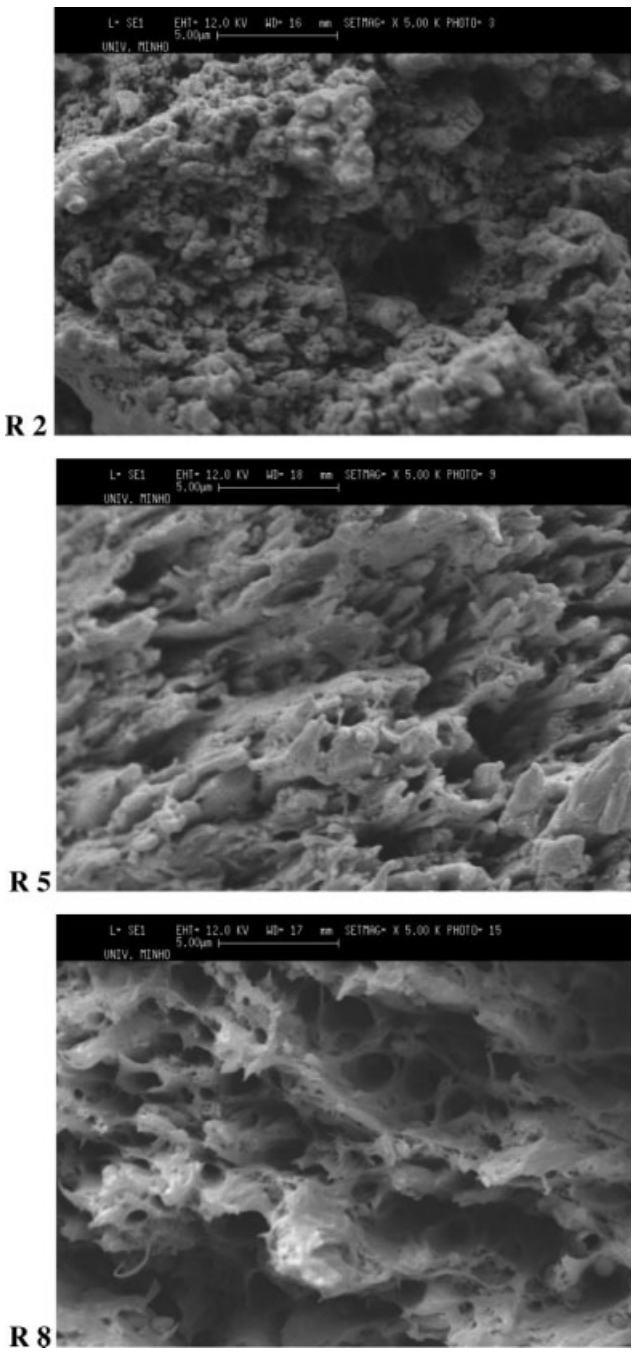

Figure 4 Magnified (×5,000) SEM micrographs of the intermediate layer for selected moldings. (R2): $T_{inj} = 220°C$; $T_w = 40°C$, $Q_{inj} = 18.4$ cm^3/s; (R5): $T_{inj} = 250°C$; $T_w = 40°C$, $Q_{inj} = 4.9$ cm^3/s; (R8): $T_{inj} = 280°C$; $T_w = 40°C$, $Q_{inj} = 27.0$ cm^3/s.

Differential scanning calorimetry

The DSC scans for all the moldings are shown in Figure 5. The degree of crystallinity of the moldings is relatively low, as expected because the room temperature PET/0.6PHB solid contains 4 phases: PET crystals, PHB-rich islands, isotropic PET-rich glass and PHB-rich glass.[33] A very small and broad crystalline peak is observed centred approximately at

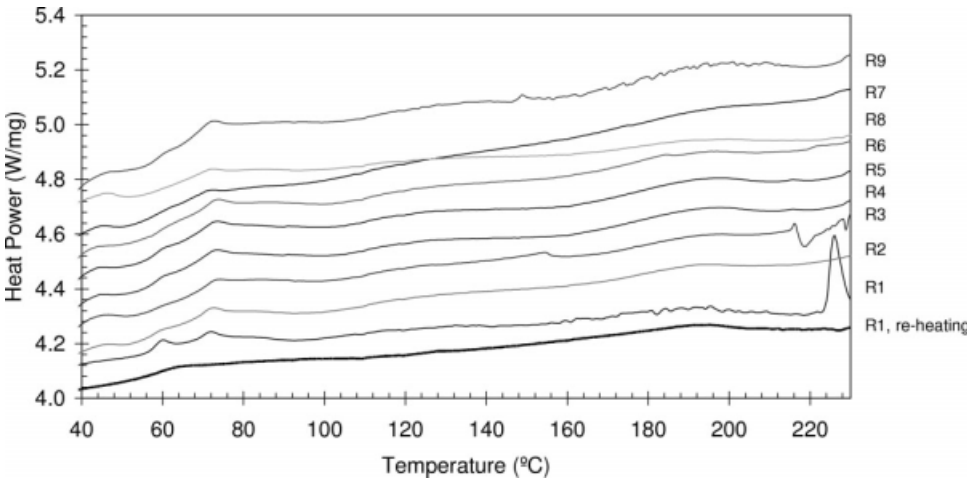

Figure 5 DSC scans for all the processing runs (see Table I for processing conditions and run identification).

190°C and ranging from approximately 150– 220°C (we recall the melting temperature resulting from a combination of results obtained by several techniques = 200°C[33] whereas that temperature from DSC alone is 212°C[10]). The calculated enthalpies of fusion are very small, of the order of 2–4 J/g, whereas the experimental errors are significant. In Ref. 1 the value of H_m = 3 J/g is reported, in the middle of our range. The low H_m value is typical for melting PLCs because the transition on heating does not result in a single isotropic phase but in a fairly well-ordered LC-containing phase.

Two glass transitions can be detected in all systems at 58 and 78°C. These processes are identified here by the endothermic peaks resulting from a structural relaxation process that occurred at room temperature before the DSC experimental run. By dynamic mechanical analysis a loss peak was found at 65°C (at 3 Hz) in PET/0.6PHB, ca. 12°C below the T_g of the pure PET.[33] Also in dielectric relaxation spectroscopy a α relaxation is identified for PET/0.6PHB at 60°C (maximum of the dielectric loss at 1 Hz), and it is attributed to the glass transition of the PET-rich domains.[39] A weak process, labelled α′, was found at approximately 40°C and was ascribed to segmental dynamics within the PHB-rich domains; apparently this mechanism was not visible in the DSC results of the present work. The presence of the α-relaxation in the PLC material was also confirmed by thermally stimulated depolarization, where a depolarization peak was observed at 65°C, and again attributed to the glass transition within the PET-rich phase.[40]

No significant differences were found in the two glass transition detected from the range of sample prepared. Second run DSC experiments were performed right after the first ones (see first lower curve in Fig. 6), to investigate the thermal properties of the samples after erasing the processing history. As

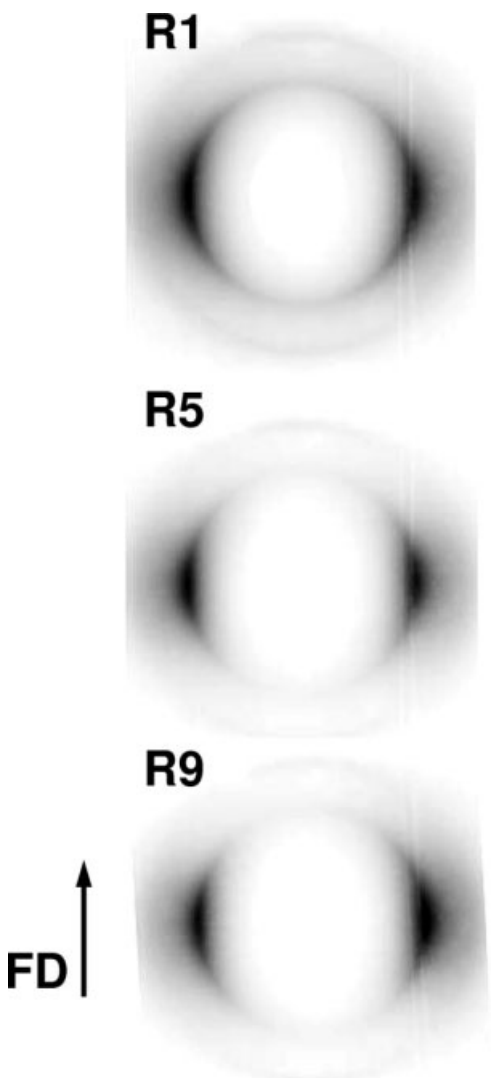

Figure 6 WAXS patterns for different processing conditions. (R1): T_{inj} = 220°C; T_w = 20°C, Q_{inj} = 4.9 cm^3/s; (R5): T_{inj} = 250°C; T_w = 40°C, Q_{inj} = 4.9 cm^3/s; (R9): T_{inj} = 280°C; T_w = 60°C, Q_{inj} = 4.9 cm^3/s. FD is the flow direction.

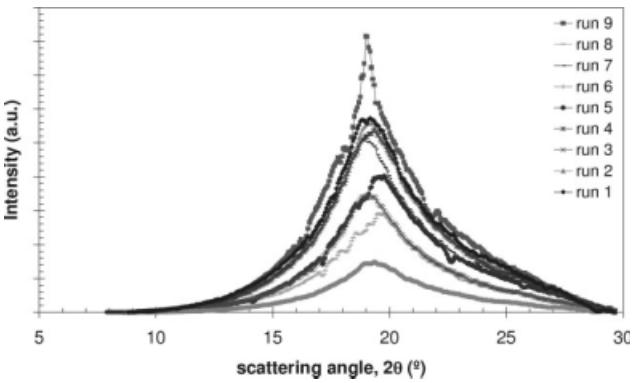

Figure 7 WAXS equatorial intensity scans for all the processing runs.

expected, the two endothermic peaks were no longer detected, as the thermal history was erased. Moreover, the high temperature glass transition process almost vanished, and only the glass transition at $\approx 58^{\circ}C$ was detected as a step in the heat flow curve. This result is consistent with the findings observed for PET/0.6PHB discussed before. The high glass transition process should be then assigned to the segmental mobility of a confined PET-rich phase, induced during the processing. The developed shear stresses may create PET-rich amorphous regions that are geometrically confined within oriented crystalline structures. The difference in the dynamics for conformational mobility of bulk-like and confined amorphous PET was already quantified[41] from a practical point of view; apparently amorphous PET entrapped within crystalline structures exhibits a higher T_g than the one found in pure amorphous PET. Interestingly, the confinement effect due to the processing studied in this work seems to be similar in both skin and core of the injected parts. Samples taken from these two regions were also tested by DSC and, in the first run, the same position in the temperature axis and similar relative intensities of the two glass transitions were observed. Another possibility for the assignment of the two glass transitions is to consider the existence of two kinds of glassy states: an isotropic one and a more ordered glass resulting from the freezing of the mesophase structure. It was proposed before that the ordered phase should be characterized by a lower T_g with respect to the amorphous one.[42] Under this picture, we could conclude from the double glass transition events observed in the DSC results that after injection molding the two glassy states could coexist, as the fast cooling in the mold could prevent the complete organization of the chains. In the second DSC run just the lower T_g is observed indicating that the previous cooling was slow enough to allow the formation of the mesophase and the formation of a ordered glassy structure.

Wide-angle X-ray scattering

WAXS patterns of selected moldings are presented in Figure 6.

All the patterns show an intense equatorial reflection, reflecting the presence of the PHB mesogenic groups. The angular dimension of this reflection and its spread are both dependent on the processing conditions. For this set of moldings the effect of the thermal level on the developed morphology is already visible: as the thermal level increases (from runs R1 to R9), the mesogen reflection becomes narrower and the angular scattering is reduced. As such, a higher level of orientation of specimen R9 is anticipated (as compared to condition R1).

Figure 7 represents the WAXS equatorial scattering scan for all the moldings. The mesogenic group reflection is centred at $2\theta = 19–20^{\circ}$.[6]

The effect of processing is noticeable. The diffraction peak gets more intense and broad (compare conditions R2 and R9). The peak position is the same, within the experimental error. The high increase of intensity of the reflection peak reflects an increase of magnitude of the relative order of the mesogenic groups (higher LC order). The increase of the peak width is related to a decrease of the mean LC crystallite size inside an island.

Figure 8 shows the WAXS azimuthal scans for the mesogen group reflection. As expected, the level of molecular orientation is higher in the flow direction (FD) for all the molding conditions. The different thermomechanical environments imposed on the melt during processing result in significant differences in the level of the molecular orientation (mainly in the FD).

Small-angle X-ray scattering

The SAXS patterns of selected moldings are presented in Figure 9.

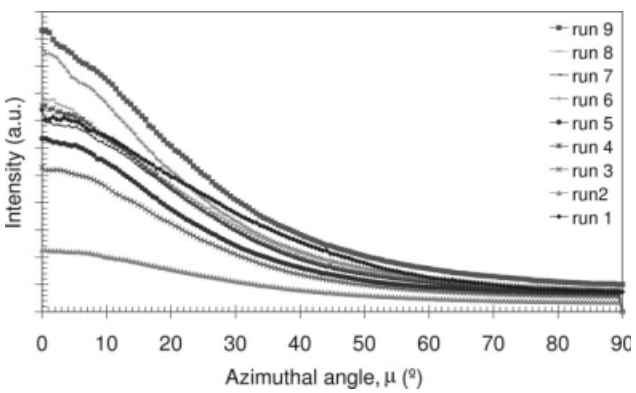

Figure 8 WAXS azimuthal intensity scans for the mesogen reflection for all the processing runs.

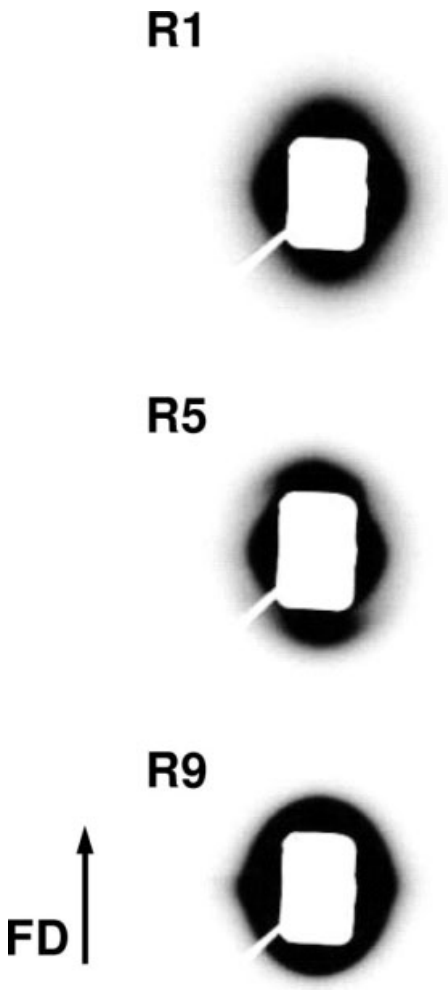

Figure 9 SAXS patterns for different processing conditions. (R1): $T_{inj} = 220°C$; $T_w = 20°C$, $Q_{inj} = 4.9$ cm^3/s; (R5): $T_{inj} = 250°C$; $T_w = 40°C$, $Q_{inj} = 4.9$ cm^3/s; (R9): $T_{inj} = 280°C$; $T_w = 60°C$, $Q_{inj} = 4.9$ cm^3/s.

The scattering pattern is typical of fibrillar morphology, with a high-long spacing and different levels of perfection. The SAXS patterns also show void scattering (voids are oriented parallel to the FD)—dependent upon the processing conditions as well. Figure 10 depicts the correspondent meridional intensity scans for all the processing runs.

The local maximum indicates some periodicity of the morphology. However, the position of this maximum is not affected by the processing conditions, showing a constant long spacing in the range from 270 to 290 nm. This value should correspond to the size of the LC-rich island. However, the perfection of this regular structure seems to be very dependent upon the thermomechanical environment imposed during processing.

The processing runs with high melt temperature (R7, R8, and R9) show more intense and well-defined peaks becasue of the development of more ordered structures. Conversely, the conditions set at low melt temperature (R1, R2, and R3) are the ones presenting broader and less intense peaks, and therefore a more heterogeneous structure.

Quantitative analysis

Table III summarizes quantitatively the morphological characterization of the moldings, in the most important measurable parameters. Processing has a pronounced effect on the layered microstructure of the moldings.

The highest variations are found in the values of (in descending order): heat capacity, intermediate skin/core layers thickness, average level of orientation. The glass transition and melting temperatures, T_g and T_m, are only slightly affected by processing. Figure 11 compares the effect of the processing conditions on the development of the morphological parameters. Run 1 shows the lowest values of s, ΔC_p, but relatively high values of the skin thickness S_i. No apparent relationship between all the morphological parameters is evident.

The variations described earlier are averaged through the molding thickness. It is expected that the morphology of each layer will also be sensitive to the applied local thermomechanical environment. A more detailed through-the-thickness characterization (layer by layer) would elucidate this point. Nevertheless, there are significant variations of the morphology induced by processing, which forecasts a distinct mechanical behavior of the moldings.

PROCESSING EFFECTS ON THE MORPHOLOGY (ANOVA)

The morphology of the moldings was found to be very sensitive to the processing conditions. Even though establishing direct links between the processing parameters (machine set), and the developed morphology of the moldings is not a satisfactory route,[32,35,36] it is important to analyze what are the

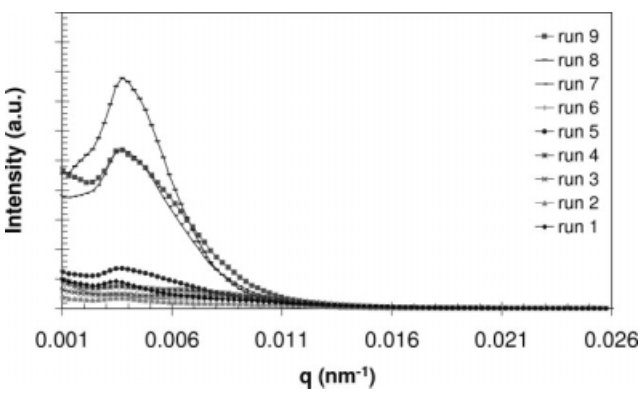

Figure 10 SAXS intensity scans for the mesogen reflection for all the processing runs.

TABLE III
Results of the Morphological Characterization

	DSC			WAXS		SEM	
Run	T_g (°C)	ΔC_p (J/g°C)	T_m (°C)	s	I_{max} (a.u.)	S_i (m/m)	C_a (m/m)
R1	67.6	0.200	191.8	0.217	0.182	0.581	0.419
R2	61.6	0.248	191.5	0.264	0.045	0.405	0.595
R3	61.9	0.226	192.8	0.325	0.097	0.541	0.459
R4	65.8	0.246	192.9	0.323	0.157	0.630	0.370
R5	63.8	0.248	192.9	0.316	0.119	0.436	0.564
R6	61.6	0.238	195.4	0.325	0.159	0.510	0.490
R7	59.1	0.330	195.3	0.326	0.146	0.566	0.434
R8	63.8	0.253	190.9	0.304	0.082	0.529	0.471
R9	63.5	0.228	194.4	0.317	0.195	0.505	0.495
Variation (%)	14.4	65.0	2.3	50.5	333.3	55.5	60.8

T_g, glass transition temperature; ΔC_p, heat capacity; T_m, melting temperature; s, level of orientation; I_{max}, maximum WAXS equatorial intensity; S_i, external layers thickness; C_a, core layer thickness.

contributions of the different processing parameters to the morphology development. Furthermore, this has been the general approach followed in the literature,[23,24,27,28] and it will be—initially—adopted in this discussion. The results were treated by analysis of variance (ANOVA). The relevant processing parameters were identified for a significance level of 0.9. The effect of processing on the microstructure of the moldings is shown in Figures 12–15.

Figure 12 represents the variations of the thickness of the external layer S_i with the processing conditions. Only T_w and Q_{inj} are significant factors. The mold temperature has the highest influence with the contribution of 71%.

S_i shows a minimum value for intermediate T_w. At the lowest T_w, the high cooling rates contribute to thicker S_i (faster cooling). For the highest T_w, the expected lower melt viscosity induces a higher level of flow-induced molecular orientation, resulting in a thicker oriented layer due to the low relaxation capabilities of PLCs.[20] This also applies to the variations of S_i with Q_{inj}; as Q_{inj} is increased, the melt viscosity decreases and the flow-induced molecular orientation increases, resulting in thicker S_i. The formation of the external layer appears to be dictated by the imposed cooling and shear levels. The negligible effect of T_{inj} may also be due to this balance. As T_{inj} increases the cooling rate decreases (lower S_i), but simultaneously the flow-induced orientation increases (higher S_i). S_i is therefore insensitive to variations of T_{inj} within the studied range. As expected, the effect of the processing conditions on the thickness of the core layer, C_a, is opposed to that of S_i.

Figure 13 depicts the evolution of the orientation parameter s with the processing variables. Generally, s increases with the increase of all the studied processing variables. The contribution of T_{inj} is the highest (c.a. 47 %). Again, the increase of the thermal level and imposed shear rate contributes to a higher molecular orientation in the moldings.

Despite the higher melt and mold temperatures, the flow-induced orientation is not allowed to relax due to the high relaxation times of PLCs. Higher Q_{inj} will decrease the melt viscosity and will enhance the orientability of the melt. The final level of molecular orientation seems to be a compromise between the orientability of the melt (related to its viscosity) and the characteristic relaxation times of the PLC, as is the case for semicrystalline polymers.[37] Furthermore, the high value of the contribution of the pooled error anticipates an eventual important interaction between the studied processing variables, as already suggested.[43] In fact, the effects of T_{inj} and Q_{inj} on the orientation levels are sometimes opposed. In general, low injection rates lead to high levels of molecular orientation,[27,42–44] but this is not always the case.[42] Higher melt temperatures result in higher levels of molecular orientation, but exceptions also exist here.[36] This reveals

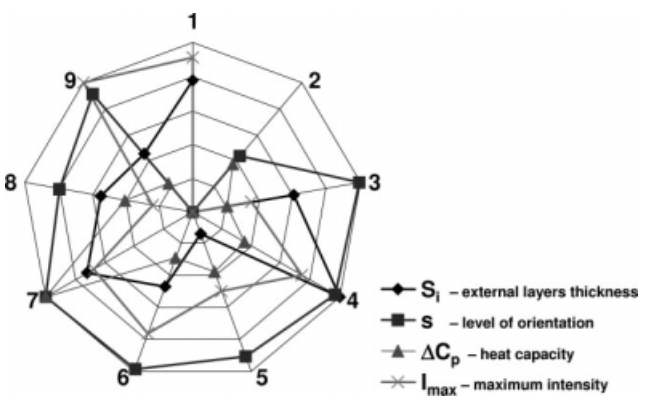

Figure 11 Effect of processing conditions on the morphological parameters (the values are normalized between 0 and 1 for comparison purposes).

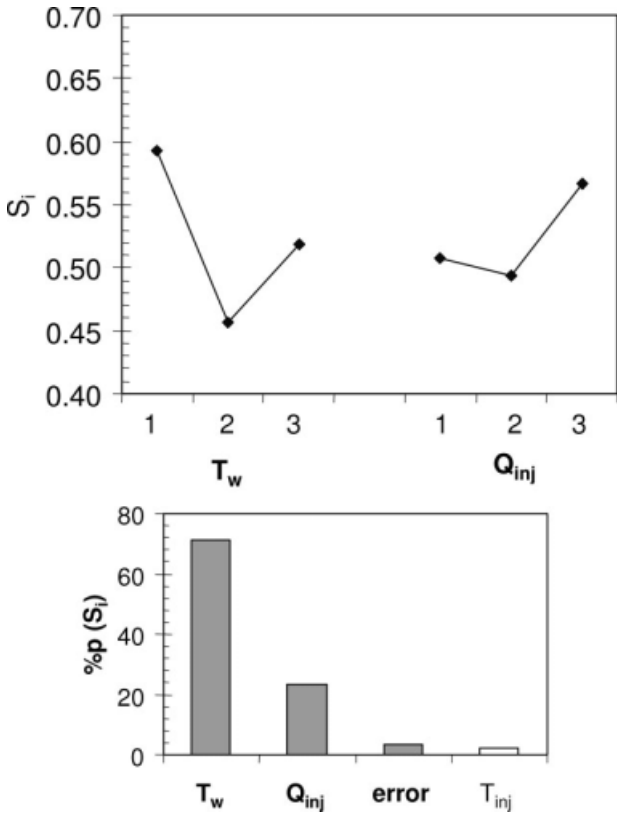

Figure 12 Effect of the processing variables on the thickness of the external layers, S_i (T_{inj}, melt temperature; T_w, mold temperature; Q_{inj}, injection flow rate; %p, percentage of contribution; error, pooled error, 1-2-3 are, respectively, the low, medium, and high level sets of the processing variables). Lines in the graph are for guidance.

some interactions between the processing parameters, their effects being a function of their relative levels. The direct link between the overall processing parameters and the morphology is therefore not a satisfactory approach.

Figure 14 represents the maximum intensity of the WAXS peak, I_{max}, as a function of the processing variables. I_{max} is proportional to the order of the LC phase: a more ordered structure gives a higher maximum intensity of the WAXS reflection.

I_{max} increases with the increase of T_{inj}, especially for the low values of this processing parameter and it also decreases with the increment on Q_{inj}, in particular for lower Q_{inj} values. The dependences of I_{max} upon T_w show a minimum value for intermediate T_w. The most important processing parameter is T_w, with the contribution of 57%, followed by Q_{inj} and T_{inj} with 27 and 12.5 %, respectively. I_{max} seems to be determined by both the cooling conditions and shear levels applied during the molding phases. A higher thermal level results in a higher level of molecular orientation as a consequence of the lower melt viscosity. Incrementing Q_{inj} leads also to a higher level of orientation, but also to a thicker skin layer resulting in a less ordered structure. The effect of T_w on the extent of order depends upon the balance between the imposed cooling and shear levels. For low T_w, the shear level is higher and for high T_w the cooling rate is lower; both these conditions leading to a higher order state. For intermediate T_w values, these opposed trends lead to low order state. Nonetheless, these relationships are not easy to establish when an average through-the-thickness I_{max} value is considered.

PROCESSING THERMOMECHANICAL ENVIRONMENT AND MORPHOLOGY RELATIONSHIPS

Clearly, the morphology development in injection molding is determined by the thermomechanical environment imposed on the melt during the processing stages. In fact, the morphology evolves inside the molding tool and is controlled locally by the thermal and mechanical fields applied to the material. Again, as already argued, it would therefore be desirable to establish relations between the local thermomechanical environment and the local morphology development.[32,35–37]

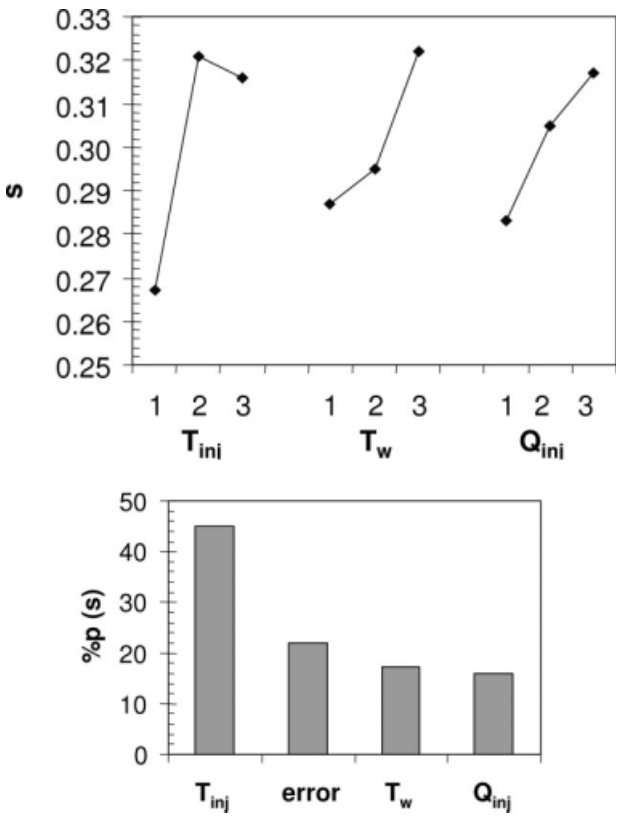

Figure 13 Variation of the level of orientation, S, with the processing variables (T_{inj}, melt temperature; T_w, mold temperature; Q_{inj}, injection flow rate; %p, percentage of contribution; error, pooled error, 1-2-3 are, respectively, the low, medium, and high level sets of the processing variables). Lines in the graph are for guidance.

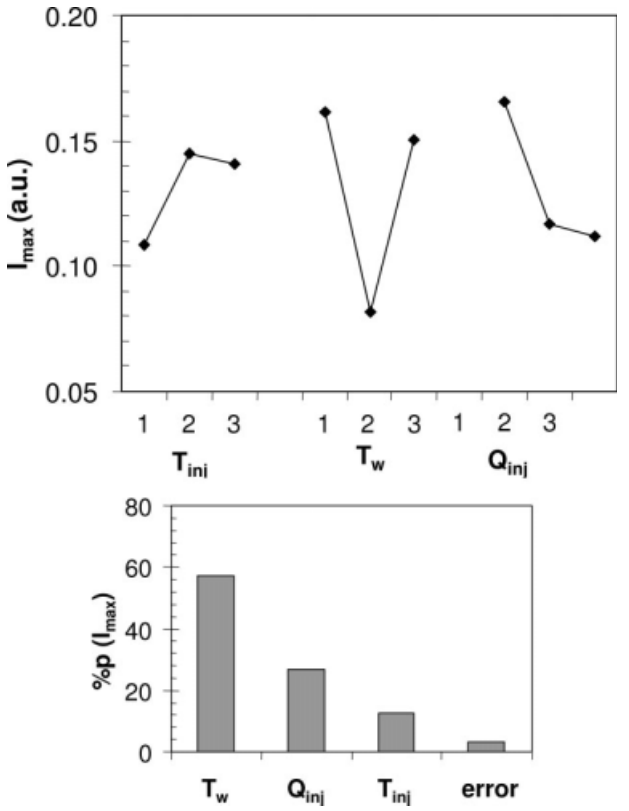

Figure 14 Effect of the processing variables on the maximum intensity, I_{max}, of the WAXS peak (T_{inj}, melt temperature; T_w, mold temperature; Q_{inj}, injection flow rate; %p, percentage of contribution; error, pooled error, 1-2-3 are, respectively, the low, medium, and high level sets of the processing variables).

Figures 15 and 16 present the variation of the assessed morphological parameters with thermomechanical variables locally computed from the mold-filling simulations. The shown dependences were chosen taking into consideration the results from previous Sections (*Processing effects – ANOVA results* and *Thermomechanical environment characterization*) and an equation that best fits the experimental data (as evaluated by the coefficient of multiple correlation, R^2, and the percentage residuals). The low values of R^2 of the fittings may indicate that other thermomechanical variables, interactions or more complex relationships need to be considered. The values of the residuals must be analysed taking into account the experimental scatter. The fitted simple equations, and the respective graphical representation, aim only at presenting the main trends of variations, evidencing the most relevant thermomechanical parameters, and their effects on the morphology development.

Figure 15 shows the variations of the outer skin ratio, S_i, with the maximum shear rate and temperature at the mold/polymer interface, T_i.

The latter is an interface temperature defined as an averaged temperature of the polymer (subscript p) and mold (subscript w) weighted by their thermal effusivities, b:

$$\mathrm{T_i} = \frac{\mathrm{b}_w \mathrm{T}_w + \mathrm{b}_p \mathrm{T}_p}{\mathrm{b}_w + \mathrm{b}_b \mathrm{p}} \tag{5}$$

Where $T_m = T_p$, $b = (\rho k c_p)^{0.5}$ (ρ is the density, K is the thermal conductivity, and c_p is the heat capacity). In this case, T_i is mainly governed by T_w.

The main processing parameters influencing S_i are T_w and Q_{inj} (Fig. 13). $\dot{\gamma}_{max}$ is mainly determined by Q_{inj} (Table II). A higher $\dot{\gamma}_{max}$ leads to a thicker oriented layer. During mold-filling, the flow-induced orientation increases with $\dot{\gamma}_{max}$. This molecular orientation cannot relax due to the long relaxation times of PLCs, thus resulting in a thicker oriented layer. Conversely, a higher T_i results in less severe cooling conditions and in a thinner external layer. The thickness of this layer seems to be related to the

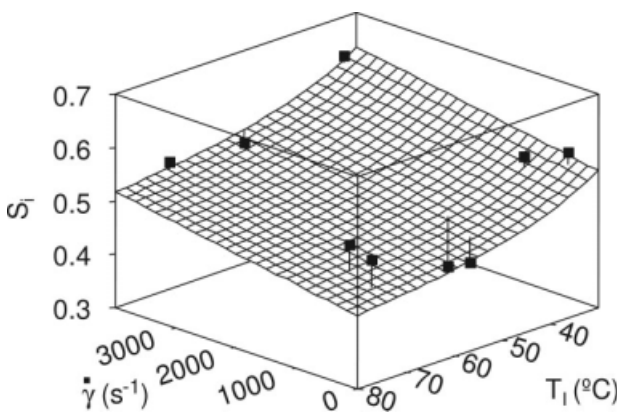

Figure 15 Effect of the thermomechanical variables on the external skin layer ratio, S_i ($\dot{\gamma}_{max}$ - maximum shear rate, T_i – interface temperature (mold/polymer), $R^2 = 0.55$; average residuals of 8.0 %; maximum residual of 23.0%).

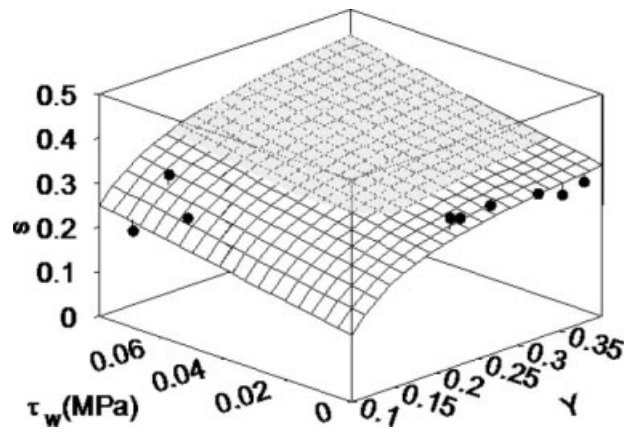

Figure 16 Effect of the thermomechanical variables on the level of orientation of the moldings, s (τ_w, shear stress at the solid/liquid interface; Y, cooling index, $R^2 = 0.71$, average residuals of 5.6 %; maximum residual of 11.0%).

shear and thermal levels – as in semi-crystalline polymers.[35,37]

Figure 16 shows the dependence of the orientation parameter s on the local shear stress and cooling index. s is affected by all processing parameters (Fig. 13). It increases with both Y and τ_w. The dependence on Y is stronger than on τ_w.

Y is mainly determined by T_{inj}. At high T_{inj} the melt viscosity is lower allowing a better melt orientability, thus, resulting in a higher flow-induced orientation. Despite the higher thermal level of the moldings, the molecular relaxation process is constrained by the high relaxation times of the rigid PLC molecules, and the flow-induced orientation is essentially preserved. The orientation parameter increases slightly with τ_w because of the strong coupling between the thermal and stress levels. In fact, the highest τ_w are obtained for the lowest Y, which tends to reduce s. On the other hand, τ_w increases also with the flow rate, Q_{inj}, contributing to an increase of the flow-induced orientation and of the final level of orientation. In Figure 16, the data points are located along a narrow area. This is due to the high coupling between the thermal and mechanical fields in the injection molding process, as mentioned earlier (Fig. 2).

CONCLUSIONS

We have established certain relationships between the local thermomechanical environment and the morphology developed in a thermotropic PLC. The main conclusions can be summarized as follows:

- A strong thermal and mechanical coupling is evidenced by the moldings.
- The imposed thermomechanical environment results in the development of a complex multilaminated and hierarchical microstructure whose thicknesses and morphological features are very sensitive to the processing conditions.
- The skin thickness is mainly determined by the mold temperature and injection flow rate, acting in opposite ways. The thickness increases with increasing melt flow shear rate and a reduction of the mold/melt interface temperature. The thickness of this layer seems to be related to the shear and thermal levels—as in semi-crystalline polymers.
- The molecular orientation increases with the increase of all processing parameters, but most significantly with the melt temperature. It is maximized for the highest thermal levels and shear stresses evidencing the preponderant effect of the flow-induced molecular orientation and high relaxation times of PLC materials.
- The order parameter (as reflected by the maximum intensity on WAXS scans) is mainly influenced by the mold temperature and injection flow rate. It seems to be determined by both the cooling conditions and shear levels applied during the molding phases.

The mechanical properties of the PLC injection moldings are expected to be determined by the morphology developed upon the constraints imposed by the processing thermomechanical environment. This will be reported later, where dependence of mechanical properties upon morphological parameters (S_i, s, and I_{max}) will be demonstrated.

References

1. Brostow, W.; Dziemianowicz, T.; Romanski, J.; Werber, W. Polym Eng Sci 1988, 28, 785.
2. Brostow, W.; Hess, M.; Lopez, B. L.; Sterzynski, T. Polymer 1996, 37, 1551.
3. Hess, M. In Performance of Plastics; Brostow, W., Ed. Hanser: Munich, Cincinnati, OH, 2000; Chapter 21.
4. Brostow, W. Polymer 1990, 31, 979.
5. Brostow, W. In Liquid Crystal Polymers: From Structures to Applications; Collyer, A. A., Ed. Elsevier Applied Science: London, 1992; Chapter 1.
6. Brostow, W., Ed. Mechanical and Thermophysical Properties of Polymer Liquid Crystals; Chapman & Hall: London, 1998.
7. Brostow, W.; Faitelson, E. A.; Kamensky, M. G.; Korkhov, V. P.; Rodin, Y. P. Polymer 1999, 40, 1441.
8. Salahshoor-Kordestani, S.; Hanna, S.; Windle, A. H. Polymer 2000, 41, 6619.
9. Vaish, N. V.; Cinader, D. K.; Burghardt, W. R.; Zhou, W.; Kornfield, J. A. Polymer 2001, 42, 10147.
10. Brostow, W.; Hibner, K.; Walasek, J. Macromol Theory Simul 2001, 10, 304.
11. Brostow, W.; Jaklewicz, M.; Montemartini, P. Mater Res Innovat 2002, 5, 261.
12. Brostow, W.; Walasek, J. J Chem Phys 2004, 121, 3272.
13. Brostow, W.; Jaklewicz, M. J Mater Res 2004, 19, 1038.
14. Samran, J. Sci Asia 1999, 15, 91.
15. Gedde, U. W.; Wiberg, G.In Mechanical and Thermophysical Properties of Polymer Liquid Crystals; Brostow, W., Ed. Chapman & Hall: London, 1998; Chapter 10.
16. Brostow, W.; D'Souza, N. A.; Kubat, J.; Maksimov, R. D. J Chem Phy 1999, 110, 9706.
17. Akinay, E. A.; Brostow, W.; Maksimov, R. Polym Eng Sci 2001, 41, 977.
18. Brostow, W.; Hess, M. Mater Res Soc Proc 1992, 255, 57.
19. Hess, M.; Lopez, B. L. In Mechanical and Thermophysical Properties of Polymer Liquid Crystals; Brostow, W., Ed. Chapman & Hall: London, 1998; Chapter 9.
20. Viola, G. C.; Baird, D. G.; Wilkes, G. L. Polym Eng Sci 1985, 25, 888.
21. Weng, T.; Hiltner, A.; Baer, E. J Mat Sci 1986, 21, 744.
22. Hedmark, P. G.; Lopez, J. M. R.; Westdahl, M. Polym Eng Sci 1988, 28, 1248.
23. Zhong, Y. In Mechanical and Thermophysical Properties of Polymer Liquid Crystals, Brostow, W., Ed. Chapman & Hall: London, 1998; Chapter 4.
24. Plummer, C. J. G.; Zulle, B.; Demarmels, A.; Kausch, H. H. J Appl Polym Sci 1993, 48, 751.
25. Brostow, W.; Triouleyre, S. Polymer 1996, 37, 1561.

26. Blonski, S.; Brostow, W.; Hess, M. Macromolecules 1993, 26, 84.
27. Zülle, B.; Demarmels, A.; Plummer, C. J. G.; Kausch, H.-H. Polymer 1993, 34, 3628.
28. Rendon, S.; Burghardt, W. R.; Bubeck, R. A.; Thomas, L. S.; Hart, B. Polymer 2005, 46, 10202.
29. Brostow, W.; Cunha, A. M.; Quintanilla, J.; Simoes, R. Macromol Theory Simul 2002, 11, 308.
30. Simoes, R.; Brostow, W.; Cunha, A. M. Polymer 2004, 45, 7767.
31. Simoes, R.; Cunha, A. M.; Brostow, W. e-Polymers 2004; no. 067.
32. Cunha, A. M.; Godinho, J. S.; Viana, J. C. In Structure Development During Polymer Processing, NATO-ASI Series, Vol. 370; Cunha, A. M., Fakirov, S., Eds. Kluwer Academic: Utrecht, 2000; p 255–277.
33. Brostow, W.; Hess, M.; Lopez, B. L. Macromolecules 1994, 27, 2262.
34. Tormes, M.; Munoz, M. E.; Pena, J. J.; Sanatmaria, A. J Polym Sci Phys 1998, 39, 253.
35. Viana, J. C. Polymer 2004, 45, 993.
36. Viana, J. C.; Billon, N.; Cunha, A. M. Polym Eng Sci 2004, 44, 1522.
37. Viana, J. C.; Billon, N.; Cunha, A. M. Polymer 2002, 43, 4185.
38. Arrighi, V.; Higgins, J. S.; Abis, L.; Weiss, R. A. Polymer 1996, 37, 141.
39. Carius, H. E.; Schnhals, A.; Guigner, D.; Sterzynski, T.; Brostow, W. Macromolecules 1996, 29, 5017.
40. Brostow, W.; Kaushik, B. K.; Mall, S. B.; Talwar, I. M. Polymer 1992, 33, 4687.
41. Alves, M. N.; Mano, J. F.; Balaguer, E.; Meseguer Dueñas, J. M.; Gomez Ribelles, J. L. Polymer 2002, 43, 4111.
42. Fernandez-Blazquez, J. P.; Bello, A.; Perez, E. Macromolecules 2004, 37, 9018.
43. Guerrica-Echevarria, G.; Eguiazabal, J. I.; Nazabal, J. Polym Test 2001, 20, 403.
44. Heynderickx, I.; Paridaans, F. Polymer 1993, 34, 4068.